LRP 705/01 Septembre 2001

Neutral beam stabilization of sawtooth oscillations in JET

C. Angioni, A. Pochelon, N.N. Gorelenkov.
K.G. McClements, O. Sauter, R.V. Budny,
P.C. de Vries, D.F. Howell, M. Mantsinen,
M.F.F. Nave, S.E. Sharapov
& contributors to the EFDA-JET
workprogramme

Submitted for publication in
Plasma Phys. & Contr. Fusion

ISSN 0458-5895

Neutral beam stabilization of sawtooth oscillations in JET

C. Angioni[1] §, A. Pochelon[1], N.N. Gorelenkov[2], K.G. McClements[3], O. Sauter[1], R.V. Budny[2], P.C. de Vries[4], D.F. Howell[3], M. Mantsinen[5], M.F.F. Nave[6], S.E. Sharapov[3] and contributors to the EFDA–JET Workprogramme†

[1]Centre de Recherches en Physique des Plasmas, Association EURATOM - Confédération Suisse,
École Polytechnique Fédérale de Lausanne, 1015 Lausanne, Switzerland
[2]Princeton Plasma Physics Laboratory, Princeton, N.J. 08543, USA
[3]EURATOM/UKAEA Fusion Association, Culham Science Centre, Abingdon, OX14 3DB, UK
[4]FOM-Instituut voor Plasmafysica 'Rijnhuizen', Associatie EURATOM–FOM, P.O. Box 1207, 3430 BE, Netherlands
[5]Helsinki University of Technology, Association EURATOM-Tekes, Espoo, Finland
[6]Associação EURATOM/IST, Centro de Fusão Nuclear, 1096 Lisbon, Portugal
†See annex of J. Paméla et al, "Overview of Recent JET Results and Future Perspectives", Fusion Energy 2000 (Proc. 18th Int. Conf. Sorrento, 2000), IAEA, Vienna (2001)

Abstract. Recent experiments in the Joint European Torus (JET) have provided evidence of sawtooth stabilization by fast ions arising from deuterium neutral beam injection. A possible theoretical basis for the interpretation of the observed sawtooth period behaviour is investigated and predictions are compared with experimental results, using a sawtooth period model developed to predict the sawtooth period in the International Thermonuclear Experimental Reactor (ITER). In this model a beam ion contribution to the internal kink potential energy has been incorporated, using a simple analytical expression valid in the limit of isotropic fast particles. This analytical expression has been validated by detailed calculations performed with a hybrid kinetic/MHD code NOVA–K, using fast particle distribution functions computed with a plasma analysis code TRANSP. The beam ion contribution has been implemented in a transport code PRETOR and a few representative JET discharges have been analyzed and modeled. The beam ion term is found to be sufficiently stabilizing to produce simulated sawtooth periods in agreement with the experimental results. Sawtooth periods computed without taking this term into account are much shorter than the measured periods. The model indicates that sawteeth are triggered in these JET discharges by excitation of the internal kink in the semi–collisional ion–kinetic regime: this was found by previous authors to be the sawtooth trigger most likely to be relevant to ITER. The role of beam ions in determining the sawtooth period in JET is thus found to be similar to the predicted role of α–particles in ITER.

§ To whom correspondence should be addressed (Clemente.Angioni@epfl.ch)

1. Introduction

Dedicated experiments have been recently performed in the Joint European Torus (JET) in order to assess the effect of fast ions arising from neutral beam injection (NBI) on sawtooth activity. Strong experimental evidence for fast ion stabilization of sawteeth has been observed during these experiments [1]. Previously, in JET tritium experiments with NBI, the sawtooth period was observed to increase with beam tritium concentration [2]: this phenomenon was attributed to a stabilizing effect of beam ions, whose energy content increased with beam tritium concentration due to the mass dependence of the slowing–down time. Analysis of internal kink stability in these discharges, in terms of thresholds given by a sawtooth period model [3], indicated that in JET hot–ion H–mode deuterium–tritium operation the contribution to the kink energy of the beam ions was greater than that of α–particles, and produced a delay in destabilization of the ideal internal kink [2].

The stabilizing effect of fast ions, in particular those arising from ion cyclotron resonance heating (ICRH), has already been investigated experimentally [4, 5] and theoretically [6, 7]. When the fast ions are produced either by ICRH or fusion reactions, the highest particle energies are in the MeV range, whereas in the case of NBI the highest energies are of the order of 100 keV. Fast particle stabilization arises from conservation of the third adiabatic invariant Φ for trapped fast particles whose bounce orbits precess around the torus in a time which is shorter than the characteristic time scale of the relevant magnetohydrodynamic (MHD) mode [6]. Modes with $m = n = 1$ have frequencies of the order of the diamagnetic frequency of thermal ions ω_{*i}, evaluated at the $q = 1$ surface. Thus, a necessary condition for fast particle stabilization is that $\omega_{Dh} > \omega_{*i}$ [6], where ω_{Dh} is the bounce–averaged toroidal precessional drift frequency of fast ions. In JET this condition is easily satisfied by ICRH ions with energies in the MeV range, even in discharges with very high ion temperature: this gives rise to delays in the sawtooth crash for periods of up to a few seconds [4, 8]. In the case of particles with energies of the order of tens of keV, on the other hand, the condition is generally only marginally satisfied.

Sawtooth stabilization by NBI fast ions was first observed in TEXTOR [9]. In those experiments, the combination of a beam injection energy ~50 keV, low densities $n_e \sim 1.5 \times 10^{19}$ m^{-3} and low ion temperatures $T_i \sim 1$ keV made it possible to stabilize sawteeth for periods of up to 200 ms. In recent discharges in JET, with beam injection at energies 80 keV and 140 keV, powers up to 10 MW, densities in the range $n_e \sim 2 - 4 \times 10^{19}$ m^{-3} and ion temperatures of a few keV ($T_i \sim 2 - 3$ keV), sawtooth periods of up to 500 ms have been observed. The ratio $\omega_{Dh}/\omega_{*i} \sim 5$ satisfies the condition for stabilization.

In order to investigate in detail the physical processes determining the period of sawtooth oscillations, we have applied a model [3] that was developed to predict the sawtooth period in the International Thermonuclear Experimental Reactor (ITER) [10]. In the model we have incorporated a beam ion contribution to the internal

kink potential energy, and compared model predictions with experimental observations. The validation of a reliable and simple sawtooth period model which can be easily combined with a one–dimensional (1D) transport code is of particular interest. Indeed, pressure profiles in tokamak plasmas can be strongly influenced by sawtooth activity, and realistic simulations and predictions of temperature and density profiles for sawtoothing discharges cannot be made purely on the basis of a transport model, but must also incorporate a model for the sawtooth period and amplitude. This is important when predicting plasma profiles in ITER: the fusion yield depends strongly on the central plasma parameters. It is envisaged that this device will have relatively high values of plasma β and, for inductive operation scenarios, low values of safety factor q at the plasma edge. In these circumstances sawtooth activity is expected to play an important role, and perhaps a favourable one, since such activity may facilitate helium ash removal. On the other hand, long sawtooth periods, such as those likely to result from α–particle stabilization in a burning plasma, can have undesirable consequences, such as the creation of seed magnetic islands capable of triggering pressure–limiting neoclassical tearing modes (NTMs) [11], or other MHD instabilities. Prediction of the sawtooth period and theoretical investigation of possible experimental tools that could be used for controlling sawtooth activity are thus of particular importance.

Preliminary versions of the sawtooth period model considered in this work have already been applied to JET plasmas, in order to simulate the sawtooth period behaviour under a variety of heating conditions [6, 12, 13]. In these previous studies, however, separate instability regimes were compared with the experimental data, and the numerical implementation of the model was not included in a transport code that could be used to compute consistently all the plasma parameters involved in the stability thresholds. In the most recent and complete version of the model [3], a sawtooth crash can be triggered by the destabilization of the internal kink in different instability regimes, which can be either ideal or resistive, depending on the values of the plasma parameters involved. The importance of considering both regimes is illustrated by experiments in the Tokamak à Configuration Variable (TCV), in which the dependence of sawtooth period on electron cyclotron resonance heating (ECRH) power and plasma shape was studied. Sawteeth were found to be triggered by the ideal internal kink at low triangularity, high elongation and otherwise by the resistive internal kink [14]. The model has also been applied to perform sawtooth period simulations of ohmic and ECRH discharges in TCV, yielding results in very good agreement with the experimental observations, and indicating that the magnetic shear and the pressure scale length at $q = 1$ play a critical role in destabilizing the resistive internal kink mode and triggering the sawtooth crash [15, 16]: this has provided, in addition, a theoretical understanding of how ECRH can be used to control the sawtooth period.

One encounters several difficulties in attempting to assess quantitatively the extent to which theoretical sawtooth period models agree with experiments, particularly NBI–heated discharges, in which the condition for fast particle stabilization is only marginally satisfied. Stability thresholds depend on time–evolving parameters which are difficult

to measure, such as the position of the $q = 1$ surface, the magnetic shear and local gradients at this surface, and the fast particle distribution function. In the absence of experimental measurements of such crucial parameters, application of the sawtooth period model requires reconstruction of the current density and safety factor profiles that are at least consistent with the available data. It is desirable that the sawtooth period model be simple enough to be used in a 1D transport code coupled to a 2D equilibrium solver.

However, simplifying the model to this extent makes it necessary to neglect additional effects, such as plasma rotation, or to simplify the description of physical effects which are taken into account. For instance one makes the assumption of isotropic distribution function in the expression describing the beam ion contribution to the internal kink potential energy. This limits somewhat the degree to which one can draw firm conclusions regarding the validity of quantitative model predictions. On the other hand, separate calculations can be performed in order to investigate the validity of the assumptions made in the modelling, and to test the simplified expressions used in the transport code, using more rigorous and complete MHD codes.

In particular, in order to check the validity of the assumption of isotropic beam ions, we have computed more realistic fast particle distribution functions, for certain specified time slices, with the post–processing transport analysis code TRANSP [17]. We have used these distribution functions as input for the hybrid MHD/kinetic code NOVA–K [18], in order to calculate accurately the contribution of beam ions to the internal kink energy and compare with estimates based on the approximate formula included in the sawtooth period model.

In the next section we describe in more detail the recent observations obtained in JET experiments. The sawtooth period model will be briefly presented in section 3. The expression used in the model for the beam ion contribution and the comparison with NOVA–K calculations are described in section 4. The beam ion kink energy contribution has been implemented in the 1-1/2 D transport code PRETOR [19], and detailed analysis and simulations of a few representative recent JET discharges have been carried out. The results are presented in section 5. The predictions of the sawtooth period model are shown to be in good agreement with the experimental results. This confirms the hypothesis that the observed time evolution of the sawtooth period is determined largely by beam ion stabilization and validates the theoretical model for quantitative predictions of the sawtooth period, at least for plasma and heating conditions similar to those prevailing in these experiments.

2. Experimental observations

Recent experiments in JET with auxiliary heating provided by NBI only have provided several indications of beam ions playing a role in stabilizing sawteeth. In particular, a NBI shot database has been built, showing an inverse correlation between the sawtooth period τ_{saw} and the electron density n_e [1, 20]. Note that the inverse density scaling of

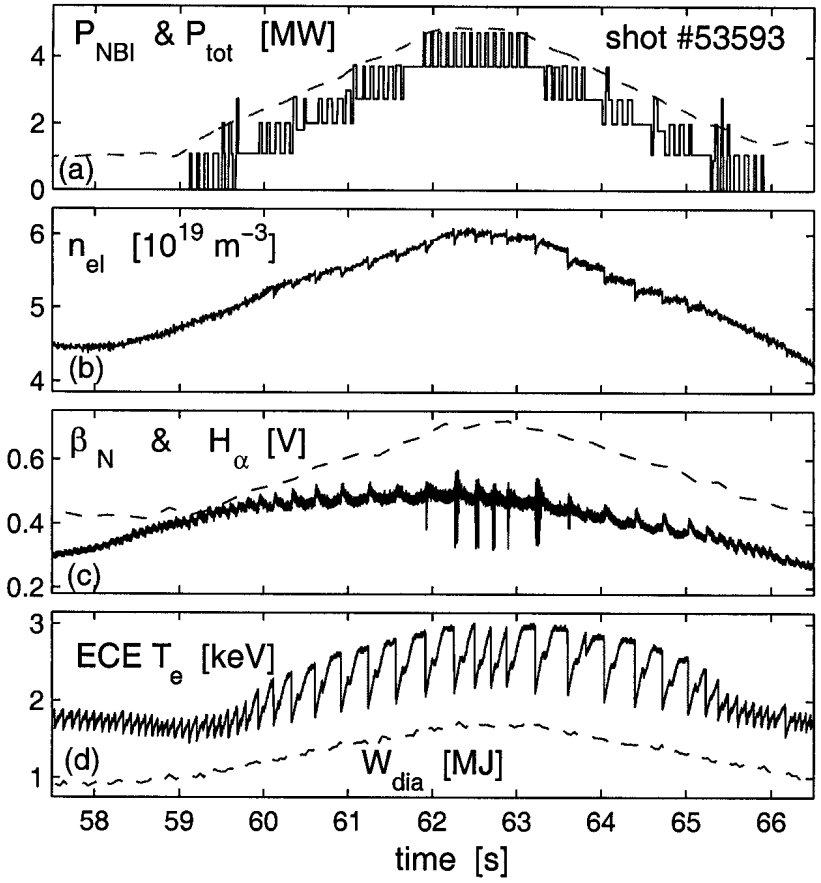

Figure 1. Experimental traces of shot ♯53593, with $I_p \simeq 2$ MA, $B_0 = 2.48$ T. (a) NBI power (solid curve) and smoothed total input power (dashed curve) in MW. (b) Interferometer central chord line–average density in 10^{19} m^{-3}. (c) H_α emission signal in V and normalized beta β_N (dashed line). (d) Electron temperature in keV (solid curve) measured by the ECE radiometer and diamagnetic plasma energy in MJ (dashed curve).

the sawtooth period is opposite to the usual ohmic behaviour, which shows an increase of $\tau_{\rm saw}$ with density. Since, under steady–state conditions, the beam ion pressure is directly proportional to the slowing–down time, which varies as $T_e^{1.5}/n_e$, it strongly suggests that the stabilization of the sawtooth period observed during NBI heating is due to fast particle effects. Moreover, the strong T_e dependence suggested by collisionality arguments is confirmed by regression analysis over the sawtooth database [21]. Work is in progress in order to identify separate dependences on temperature, density and NBI power.

The dedicated experiments considered in the present analysis have been performed with relatively slow NBI power (P_{NBI}) ramps, in order to obtain sawtooth period data over a wide power range. The NBI power has been rapidly modulated in order to optimize the simulation of a continuous linear variation in time, with a power range up to almost 10 MW. Higher power levels have not been considered, since other instabilities,

such as fishbones, would then be expected to occur, thereby complicating the sawtooth analysis.

In figure 1 we show an overview of shot ♯53593, with plasma current $I_p = 2$ MA, safety factor $q_{95} \simeq 4$, and vacuum magnetic field $B_0 = 2.48$ T. The modulated trapezoidal power waveform is shown in figure 1(a), together with the smoothed total input power, which includes also the ohmic contribution. In this shot the low maximum $P_{NBI} < 5\,\mathrm{MW}$ and the relatively high magnetic field keep the plasma in L–mode throughout the heating phase, with a resulting line–averaged density, plotted in figure 1(b), whose waveform roughly follows the NBI power waveform. The H_α emission signal is shown in figure 1(c), together with $\beta_N = \beta[\%]\, a[m]\, B_0[T] \,/\, I_p[MA]$, a being the minor radius and $\beta[\%]$ the ratio of volume–averaged pressure to toroidal field pressure at magnetic axis, expressed in percentage. In figure 1(d) we have plotted the electron temperature measured by the electron cyclotron emission (ECE) heterodyne radiometer. The present time trace corresponds to a point of the plasma which is located, from magnetic equilibrium reconstruction, approximatively at $r/a \simeq 0.13$, roughly 50% inside the inversion radius. The sawtooth period increases with increasing power already at these low power levels. Figure 1(d) shows also the plasma diamagnetic energy.

In all these experiments, the beams are in the co–direction, and therefore plasma rotation increases with NBI power. The beam trajectories, in the JET upshifted alignement, allow a strong localization of the power absorption and of the fast particle pressure in the central region of the plasma. This is particularly important in order to obtain a visible effect of fast particles on the sawtooth period, since, from theory, the most important parameter determining sawtooth stabilization is roughly given by the volume–averaged fast particle energy content inside the $q = 1$ surface with respect to the value of the fast particle energy at that surface.

Both simple ramp-up followed by a rapid drop or trapezoidal P_{NBI} waveforms, involving power ramp-up and ramp-down with the same time scales have been analyzed. A linear relation between the sawtooth period and the fast ion energy content $W_{i\,fast}$ has been observed in all the discharges. Moreover, the plot of the evolution of the sawtooth period versus the NBI power exhibits a hysteresis behaviour as P_{NBI} rises and decays, which is slightly reduced when τ_{saw} is plotted versus the energy content $W_{i\,fast}$ [1]. This suggests that the variations in τ_{saw} are better correlated with changes in $W_{i\,fast}$ than with changes in P_{NBI}, supporting the idea that fast ions are responsible for sawtooth stabilization.

3. Sawtooth period model

In this section we present a brief overview of the sawtooth period model, using the notations and normalisations adopted in [3]. The dimensionless internal kink energy functional $\delta\hat{W}$ is defined such that, in the ideal MHD limit, $\delta\hat{W} = -\gamma\,\tau_A$, where γ is the growth rate and $\tau_A = \sqrt{3}R_0/c_A$, R_0 being the major radius and $c_A = B_0/(\mu_0 n_e m_i)^{1/2}$ the Alfvén speed (m_i is the ion mass and μ_0 the free space permeability). Quantities

evaluated at the $q = 1$ surface are indicated by the subscript "1".

In the presence of a fast particle population, whose related parameters are indicated with the subscript "h", a sawtooth crash is assumed to occur when any one of the following conditions is satisfied [cf. equations (13), (14) and (15) in [3]]

$$-\delta\hat{W}_{core} > c_h\,\omega_{Dh}\,\tau_A, \tag{1}$$

$$-\delta\hat{W} > 0.5\,\omega_{*i}\,\tau_A, \tag{2}$$

$$-c_\rho\,\hat{\rho} < -\delta\hat{W} < 0.5\,\omega_{*i}\,\tau_A \tag{3a}$$

$$\text{and} \quad \gamma_{\text{eff}} > c_r\,(\omega_{*i}\omega_{*e})^{1/2}. \tag{3b}$$

These stability thresholds are applicable provided that the auxiliary condition $\omega_{Dh} > \omega_{*i}$ is satisfied, where ω_{Dh} is of the order of $cE_h/(4eB_0R_0r_1)$ and the diamagnetic frequency $\omega_{*i} = (dp_i/dr)|_{r=r_1}/(en_eB_0r_1)$, $-e$ being the electron charge.

In equation (1), $\delta\hat{W}_{core} = \delta\hat{W}_{MHD} + \delta\hat{W}_{KO}$ is the core plasma component of $\delta\hat{W}$. When this equation is satisfied, high energy ions have an insufficient stabilizing influence: a sawtooth crash is triggered if the internal kink growth rate $-\delta\hat{W}_{core}/\tau_A$ is larger than $c_h\omega_{Dh}$, where c_h is a numerical factor of order unity. Following [3], we set this factor equal to 0.4. $\delta\hat{W}_{MHD}$ is the ideal MHD term, including effects of toroidicity and plasma shape [22], and $\delta\hat{W}_{KO}$ is the Kruskal–Oberman term [23], which takes into account the effects of collisionless trapped thermal ions (they are usually strongly stabilizing). Analytical expressions for these terms can be found in Appendix B of [3].

The second sawtooth trigger criterion [equation (2)] is that the internal kink growth rate $\gamma \simeq -\delta\hat{W}/\tau_A$ be sufficiently large to overcome stabilization due to thermal ion diamagnetic effects. Fast particle effects are included in the potential energy functional $\delta\hat{W}$ by means of the additional term $\delta\hat{W}_{fast}$:

$$\delta\hat{W} = \delta\hat{W}_{MHD} + \delta\hat{W}_{KO} + \delta\hat{W}_{fast}. \tag{4}$$

The explicit expression used for the term $\delta\hat{W}_{fast}$ will be discussed in the next section. When either equation (1) or (2) are satisfied the internal kink is unstable and has a structure similar to the ideal mode. Therefore it will be referred to as the ideal internal kink in the following.

When the mode dynamics and linear growth rate are determined by microscopic effects in a narrow layer, equation (3), the mode is modified and will be referred to as a resistive internal kink. In equation (3a), c_ρ is a numerical factor kept equal to 1, and $\hat{\rho} = \sqrt{\rho_i^2 + \rho_s^2}\,/\,r_1$ where ρ_i is the thermal ion Larmor radius and ρ_s is the same quantity evaluated using the electron temperature rather than the ion temperature [note that in [3] there is a misprint in the definition of $\hat{\rho}$, after equation (6)]. Quantities appearing in equation (3b) will be defined below. When the stabilizing effects are strong enough that $-\delta\hat{W} < -c_\rho\,\hat{\rho}$, which is often the case when fast particles are present, the mode structure changes its nature, from a global resistive internal kink to a drift–tearing mode [24], strongly localized near the $q = 1$ surface, and assumed not global enough to trigger a sawtooth crash.

When equation (3*a*) is satisfied, layer physics around the $q = 1$ surface plays the crucial role. In equation (3*b*) γ_{eff} is the maximum growth rate of the resisitve internal kink, in our case $\gamma_{\text{eff}} = \max(\gamma_\rho, \gamma_\eta)$, depending on the dominant layer width. The reconnection layer width is in general determined by either the resistive layer width δ_η (defined below) or by the ion thermal Larmor radius ρ_i: depending on the values of these length scales, the resistive internal kink can be destabilized in the following different instability regimes.

If $\delta_\eta > \rho_i$, finite resistivity makes it possible for the internal kink mode to become unstable in the resistive regime, with a growth rate given by

$$\gamma_\eta = s_1^{2/3} S^{-1/3} / \tau_A, \tag{5}$$

where s_1 is the magnetic shear evaluated at the $q = 1$ surface, and $S = \tau_\eta/\tau_A$, the magnetic Reynolds (Lundquist) number, with $\tau_\eta = \mu_0 r_1^2/\eta$ the resistive diffusion time (η being the resistivity). In terms of these quantities, the resistive layer width δ_η is equal to $s_1^{-1/3} S^{-1/3} r_1$.

If, on the other hand, $\rho_i > \delta_\eta > c/\omega_{pe}$, where c is the speed of light and ω_{pe} is the electron plasma frequency, the reconnection layer width is determined by ρ_i, and electron inertia can be neglected in the generalized Ohm's law. This is referred to as the semi–collisional ion–kinetic regime. The resistive internal kink growth rate is then given by [25]

$$\gamma_\rho = \left(\frac{2(1+\tau)}{\pi}\right)^{2/7} \hat{\rho}^{4/7} S^{-1/7} s_1^{6/7} / \tau_A, \tag{6}$$

where $\tau = T_{e1}/T_{i1}$. During the NBI heating phase of the discharges considered here, $\rho_i(\sim 0.4\text{cm}) > \delta_\eta(\sim 0.2\text{cm})$, and therefore the ion–kinetic regime applies.

These reconnecting modes become unstable when the growth rate exceeds a finite value determined by diamagnetic effects: this is represented by equation (3*b*), first proposed as a sawtooth trigger condition in [15] and subsequently shown to be successful in modelling the sawtooth period in ohmic and ECRH discharges in TCV [15, 16]. In this inequality, ω_{*e} is the electron diamagnetic frequency and c_r is a dimensionless numerical factor. Since both growth rates γ_η and γ_ρ involve s_1, the triggering condition can be rewritten in the form

$$s_1 > s_{1\,\text{crit}}, \tag{7}$$

where $s_{1\,\text{crit}}$, the critical shear at $q = 1$, is given by different expressions depending on whether the non–ideal internal kink is destabilized in the resistive or ion–kinetic regimes. In both cases there is a strong dependence on the local plasma parameters at $q = 1$.

The numerical factor c_r also depends on plasma parameters: in particular, it depends on the collisionality regime. In the collisionless limit $c_r \sim 1$, while in the limit of strong collisionality $c_r \simeq (D/9)^{1/3}$ [26] where D, the ratio of resistive time to perpendicular ion momentum diffusion time, is approximately equal to $0.3\beta_{e1}\sqrt{m_i T_e/m_e T_i}$, with $\beta_{e1} = n_{e1}T_{e1}/(B_1^2/2\mu_0)$. At the beginning of the NBI heating phase of the discharges considered here, the plasma is usually in a regime of low

collisionality, with ν_{e*} (the ratio of trapped electron bounce time to collision time) at $q = 1$ having values within 0.5 and 1. Later during the NBI power ramp–up, at higher temperatures but also higher densities, ν_{*e} decreases slightly, reaching values around $0.1 - 0.2$. In [3] $c_r = 1/3$ was chosen on the grounds that it was consistent with the collisionality regime predicted for ITER. In the simulations of JET NBI discharges reported here, c_r was set equal to 0.5: this is appropriate for the weakly collisional regime of these discharges.

Destabilization of a reconnecting internal kink mode, in either the resistive or ion–kinetic regime, can be determined by different triggers, depending on which condition in equation (3) is the last to be fulfilled: this can influence in different ways the duration of a sawtooth period. When equation (3*a*) is satisfied during the sawtooth ramp, a crash is later triggered when the reconnecting mode drive is strong enough to offset stabilizing diamagnetic effects: this corresponds to s_1 exceeding the critical shear [equation (7)]. On the other hand, if the condition $s_1 > s_{1\,crit}$ is fulfilled when $-\delta\hat{W}$ is still below $-\hat{\rho}$, then condition $-\delta\hat{W} > -\hat{\rho}$ determines the time of the crash. This latter situation was found in [3] to be the one most likely to be relevant for ITER operation, where the strong stabilizing effect of α–particles makes it possible for $-\delta\hat{W}$ to be less than $-\hat{\rho}$ during the sawtooth ramp. In Sec. 5 we show that this is the situation occurring in JET during the NBI heated discharges, with the role of α–particles in ITER being played by NBI fast ions in JET.

After a sawtooth crash is triggered, the profiles are relaxed according to the Kadomtsev complete reconnection model. The safety factor and current density profiles are modified up to the mixing radius, in particular yielding $q = 1$ on the magnetic axis, and $q > 1$ everywhere else along the minor radius. The density and pressure profiles are flattened within the mixing radius, with total particle number and energy conserved. The simulated sawtooth period turns out to be sensitive to the adopted profile relaxation model, particularly when the sawtooth period is comparable with the confinement time, as it is in the discharges considered in the present work.

Incomplete reconnections, yielding a post–crash safety factor profile with q below 1 on the magnetic axis and a low local shear at the $q = 1$ surface, imply that the next crash trigger is reached after a sawtooth period which is shorter than that occurring after a complete reconnection [3]. The computed time evolution of the parameters involved in the stability thresholds during the sawtooth ramp shows that a crucial role is played by the value of the shear at the $q = 1$ surface, particularly when the trigger conditions are those of equation (3). However, partial relaxations of the safety factor profile, even though they imply shorter values of $\tau_{\rm saw}$, do not change the global dependence of the sawtooth period on the plasma parameters. Sawtooth period simulations obtained assuming systematic post–crash incomplete reconnections can thus be consistently reproduced with the complete reconnection model, provided that the free parameters of the sawtooth period model, in particular c_ρ in equation (3*a*) and c_r in equation (3*b*), are rescaled. In this sense, the validity of the present analysis is not contingent on whether reconnection is partial or complete.

4. Numerical computation of $\delta\hat{W}_{fast}$ and validation of an analytical expression

In order to compute accurately the contribution $\delta\hat{W}_{fast}$ of beam ions to the internal kink potential energy, we have used the NOVA–K code [18, 27], developed to study low-n kinetic-MHD instabilities, and already used to calculate the nonadiabatic resonant response of fast particles to a given eigenmode structure. The code has been extended in order to evaluate the full fast particle response to the internal kink mode [28]. A perturbative method is used to compute the kinetic effects, while the ideal eigenmode structure is computed by the ideal MHD code NOVA. The perturbative approach is justified, since the fast particle beta on–axis, $\beta_{0\,fast}$, is about 30% of the plasma β_0 in the NBI experiments considered in the present work. The code includes fast ion finite orbit width and finite Larmor radius effects in the kinetic contribution to the MHD quadratic form of the mode energy, provided by the various fast particle groups. The code takes into account the realistic flux surface geometry and the plasma rotation profile. This is particularly important in order to describe properly the fast particle toroidal precession, and estimate correctly the precession drift frequency of the banana orbits. The code is particularly well–suited to this kind of application. Moreover, NOVA–K can be run taking as input realistic numerical calculations of the fast particle distribution function, both in energy and pitch–angle.

It is important to use a realistic form of the distribution function in order to estimate correctly the stabilization effect, since it is primarily due to trapped particles. This also tests the validity of analytical approaches to the problem. The distribution function was taken from the TRANSP Monte–Carlo package and fitted into a factorised form $f_f = f_v f_{P_\varphi} f_\chi$, where v is speed, P_φ is canonical toroidal momentum, and $\chi = (v_\perp^2/v^2)(B_0/B)$, $v_\perp$ denoting the velocity component perpendicular to the local magnetic field B. The factor f_{P_φ} represents essentially the radial dependence of the distribution, and was taken from the TRANSP code [17]. The speed distribution f_v is assumed to be slowing–down, which is also supported by TRANSP modelling. For the NBI ion pitch–angle distribution f_χ, we used the form

$$f_\chi = e^{-(\chi-\chi_0)^2/\Delta_\chi^2}, \tag{8}$$

which gives the distribution function in the equatorial plane at the low field side. Comparison with the TRANSP code shows that it can be assumed that $\chi_0 \simeq 0.5$ within the numerical accuracy, and it has been verified not to change significantly within the $q = 1$ surface. The pitch–angle width depends strongly on the particle energy, and must be computed from the collisional operator in the Fokker–Planck equation [29], which also determines the speed of a particle as it slows down:

$$v^3 = \left(v_{cr}^3 + v_{b0}^3\right) e^{-3t/\tau_{se}} - v_{cr}^3. \tag{9}$$

Here v_{b0} is the beam injection speed and v_{cr} is the speed at which a beam particle slows down on ions and electrons at the same rate. The collisional pitch–angle scattering diffusion coefficient has the form $D_{\chi\chi} = v_{cr}^3/(v^3\,\tau_{se})$, and the pitch–angle width at a

specific time t is $\Delta_\chi^2 = \Delta_0^2 + \int_0^t D_{\chi\chi} dt$, where particle speed must be treated as a function of time, according to equation (9). It is straightforward to show that

$$\Delta_\chi^2 = \Delta_0^2 + \frac{1}{3} \ln \left[\frac{v^3 \left(1 + v_{cr}^3 / v_{b0}^3\right)}{v^3 + v_{cr}^3} \right]. \tag{10}$$

Like the parameter χ_0, also Δ_0 can be easily determined from the distribution functions given by TRANSP.

Figure 2 shows the sensitivity of the fast particle contribution $\delta\hat{W}_{fast}$ to the width Δ_χ of the pitch–angle distribution. With open circles we have plotted the code results including finite Larmor radius (FLR) effects, whereas open squares indicate the excess of stabilization obtained when FLR effects are neglected. Two different behaviours can be identified: with a localized distribution function in pitch–angle, roughly $\Delta_\chi < 1$, $\delta\hat{W}_{fast}$ shows a strong dependence on Δ_χ, while for $\Delta_\chi > 1$, $\delta\hat{W}_{fast}$ becomes almost a constant function of $\Delta\chi$, rapidly reaching the isotropic limit. The distribution functions fitted from the TRANSP results have in general pitch–angle widths which turn out to be complicated functions of both the normalized poloidal flux averaged over the particle trajectory $\psi = \psi(\chi, P_\varphi, v)$ and of the particle energy $\mathcal{E}$. For example, for a specific time of the JET discharge ♯53595 at which the TRANSP distribution was computed, the fitting expression for the pitch–angle width used as input for NOVA–K was

$$\Delta_\chi^2 = 0.13 + 0.45\sqrt{\psi} \; - \; 0.15 \ln \left[\frac{(\mathcal{E}/130)^{3/2} \left(1 + 0.729\right)}{(\mathcal{E}/130)^{3/2} + 0.729} \right],$$

where $\mathcal{E}$ is expressed in keV. The corresponding value $\delta\hat{W}_{fast} = 2.74\ 10^{-3}$ computed with this distribution function, fitted from the TRANSP result for this specific time, is shown by a tick at the right hand side of figure 2 and by a dotted horizontal line. This allows us to identify an "effective" value of the pitch angle width $\Delta_\chi \simeq 0.3$, where this horizontal line crosses the curve with open circles. This example shows that the "effective" pitch–angle widths corresponding to the experimental conditions are in general in the region in which $\delta\hat{W}_{fast}$ varies strongly with Δ_χ. This implies that numerical calculations properly taking into account the realistic distribution function are indeed necessary. In figure 2 we have also marked the corresponding value $\delta\hat{W}_{fast} = 2.56\ 10^{-3}$ provided by the analytical formula [30, 31]

$$\begin{aligned} \delta\hat{W}_{fast} &= -\frac{\beta_{0\,fast}}{\sqrt{2} s_1 \epsilon_1^{1/2}} \int_0^{r_1} \left(\frac{r}{r_1}\right)^{3/2} \frac{d\hat{p}_{fast}}{dr} dr \\ &= \frac{\sqrt{2}\,\mu_0\,\epsilon^{3/2}}{s_1} \left[\langle \left(\frac{r_1}{r}\right)^{1/2} p_{fast} \rangle_{q=1} - p_{fast}(r_1) \right], \end{aligned} \tag{11}$$

where $\beta_{0\,fast}$ is the toroidal fast ion beta at the magnetic axis and $\hat{p}_{fast}(r)$ is the normalized fast ion pressure profile. The present formula for $\delta\hat{W}_{fast}$ involves a weighted volume–averaged pressure of the fast particles inside the $q = 1$ surface and thereby can be written in a form which is analogous to that included in the ideal MHD term [22], involving the volume–averaged total plasma pressure inside the $q = 1$ surface. Equation

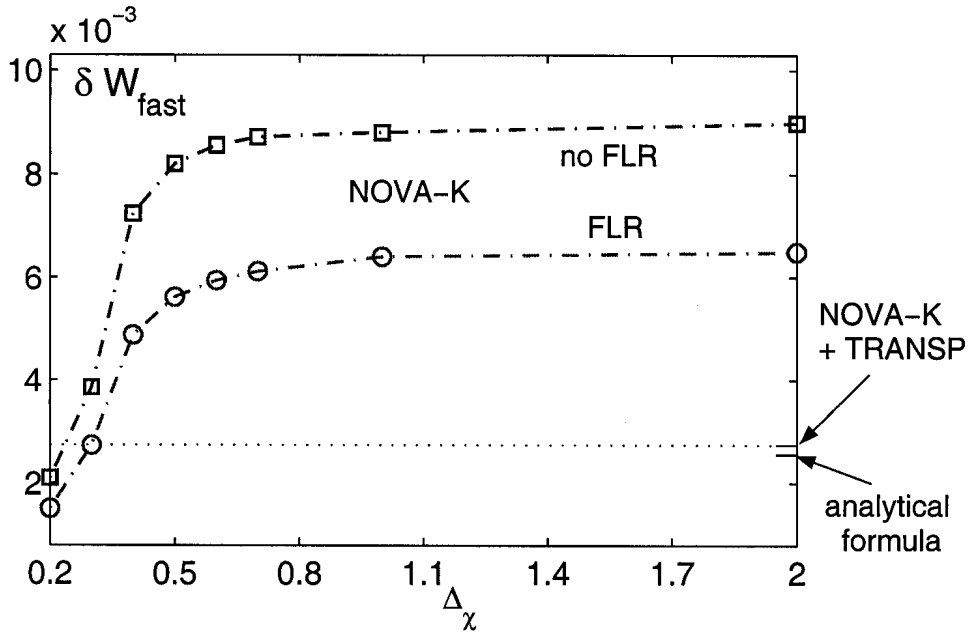

Figure 2. NOVA–K results, showing the fast particle stabilizing contribution $\delta\hat{W}_{fast}$ to the $m = 1$ internal kink potential energy, for different values of the fast ion pitch–angle distribution width [equation (8)]. Circles and square symbols give the NOVA–K results obtained respectively with and without the inclusion of finite Larmor radius effects. The fast ion distributions in energy and space were taken from the results of a TRANSP run corresponding to a specific time slice of a JET discharge (shot ♯53595). The ticks on the right hand side mark the value computed by NOVA–K taking into account the TRANSP pitch–angle distribution and the value computed with the analytical expression [equation (11)].

(11) is valid in the limit $1 - q \to 0$ and magnetic shear $s \to 0$ inside the $q = 1$ surface, for an isotropic distribution of energetic ions and without FLR effects.

The analytical expression clearly underestimates the contribution of fast particles, when compared with NOVA–K results obtained with large Δ_χ values, i.e. in the isotropic limit. This is partly due to the fact that in NOVA–K only co–going particles, in the direction of the plasma current, have been considered, consistently with the experimental set–up. Taking into account both co and counter injected beams, the fast particle contribution in the isotropic limit is reduced from 6.49 10^{-3} to 4.74 10^{-3}, which reduces the discrepancy with the analytical formula to less than a factor of 2. Moreover, NOVA–K uses realistic magnetic geometry and includes rotation effects, which may account for the remaining difference. On the other hand, it turns out that the analytical evaluations are very close to the NOVA–K results obtained using the realistic fast particle distribution function computed by TRANSP. This can be explained considering that, since the pitch–angle distribution is narrower at higher energies, fewer trapped fast ions contribute to the stabilization than in the case of an isotropic distribution. We have performed several NOVA–K runs, for specified time slices at different levels of NBI heating power, considering both an isotropic distribution function and the realistic

distribution computed by TRANSP. These calculations have shown that in general equation (11) underestimates the term $\delta\hat{W}_{fast}$ by a factor of about 3 if compared to the results provided by NOVA–K with isotropic distribution functions, but provides a surprisingly good estimate, within 15%, of the fast particle contribution when the realistic distribution functions are taken into account. This makes it possible to use equation (11) to describe the effect of fast particles on the internal kink in similar JET discharges with NBI heating, when performing simulations of the sawtooth period with a transport code such as PRETOR.

The coupling of PRETOR with an MHD code such as NOVA–K at each time–step of the transport simulation would require a prohibitive amount of computation time. The formula given in equation (11) is straightforward to include in a transport code, as it involves only the global beam ion pressure profile, together with variables such as the shear and inverse aspect ratio at $q = 1$ which are routinely computed using transport codes. This approach can be extended to other heating schemes producing fast ions in the plasma, such as ICRH. In this case the fast ion distributions are generally more complex than those resulting from NBI, in both velocity and coordinate space, and require more complicated analytical descriptions [32, 33]. In principle these analytical distributions can be benchmarked against the results of rigorous numerical modelling, carried out using interfaced Monte–Carlo codes. The simulations presented in the next Section use fast ion pressure profiles computed by a steady–state Fokker–Planck code PENCIL [34]. This is a post–processing code for JET discharges, run on a regular basis to determine the NBI heating power absorbed by the plasma, the particle sources, and the beam ion pressure profiles. By computing the fast ion pressure profile from a steady–state solution of the Fokker–Planck equation, time–dependent effects arising from the finite slowing–down time are neglected. The slowing–down time of beam ions in these JET discharges is usually between 50 and 100 ms, while in the NBI power ramp–up experiments considered here the characteristic time of the power ramp is of the order of 1 s. The use of a steady–state Fokker–Planck equation to compute the fast ion pressure is thus justified. The slowing–down time is also smaller than the energy confinement time, which is of the order of 200 ms in the discharges considered here.

5. Comparison between theory and experiment

In order to identify the relevant stability thresholds, we have computed the time evolution of all the quantities involved in the sawtooth period model, taking data directly from the available JET diagnostics and post–processing codes such as PENCIL. We have analyzed in this way five discharges, with NBI power ramps, performed in recent JET campaigns, with different NBI power levels, with a L–H mode transition or remaining in L–mode during the NBI heating phase. Figure 3 shows the results of this analysis for two shots, ♯50725 during the power ramp–up phase, before the occurrence of fishbones, and ♯53593, with lower maximum power, with a complete trapezoidal power waveform. For all the time slices, we have considered a safety factor profile, and the corresponding

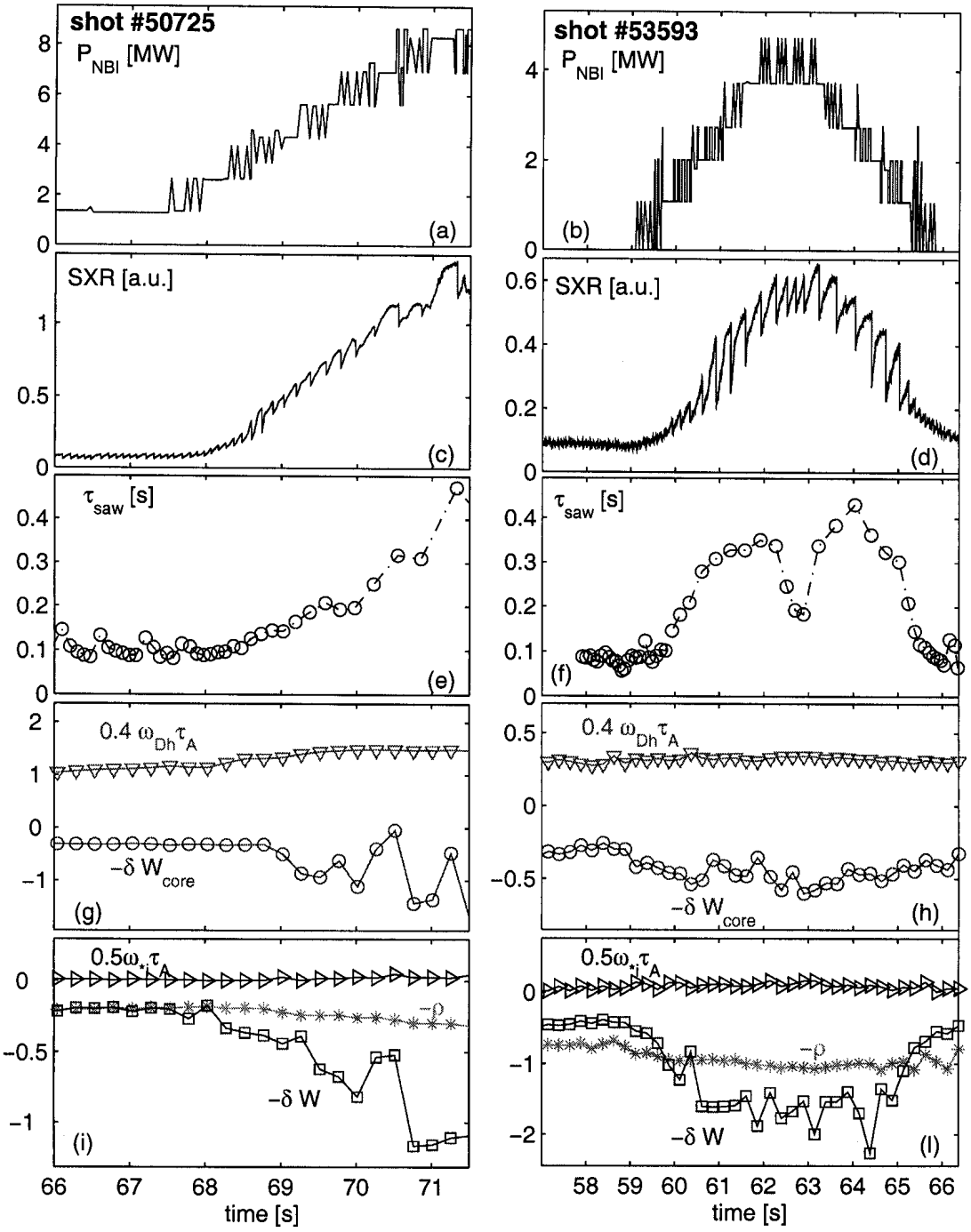

Figure 3. (a) and (b) NBI power for shots 50725 and 53593; (c) and (d) central chord Soft X–ray signals; (e) and (f) corresponding sawtooth periods; (g) and (h) stability threshold described by equation (1); (i) and (l) relevant stability threshold terms in equations (2) and (3), used in the sawtooth period model. All the terms are computed directly from experimental measurements, as described in Sec. 5, using the q profile reconstructed with PRETOR. In (g) – (l) symbols indicate time slices of the experimental measurements; $0.4\,\omega_{Dh}\,\tau_A$ is plotted with triangles pointing down, $0.5\,\omega_{*i}\,\tau_A$ with triangles pointing right, $-\delta\hat{W}_{core}$ with circles, $-c_\rho\hat{\rho}$ with stars, and $-\delta\hat{W}$ with squares.

current density profile, computed using an equilibrium reconstruction which is consistent with the experimental pressure profiles. The inversion radius has been experimentally determined for all the sawtooth crashes and used as a constraint on the reconstructed safety factor profile. We have assumed a constant "average" value of the safety factor in the center $q_0 = 0.9$. In this way we have computed the instability thresholds taking data the most directly as possible from the experimental measurements, considering the measured profiles as the ones occurring on average at the middle of a sawtooth ramp. Thus we have evaluated the order of magnitude of the different terms occurring in the sawtooth crash trigger conditions [equations (1,2,3)] at various phases of the discharges. The safety factor profiles, computed as previously described by the equilibrium code coupled with PRETOR, and which play a crucial role in sawtooth calculations, compare also very well with measurements provided by motional Stark effect diagnostics, when these are available.

In figure 3(a) and (b) we have plotted the time evolution of the heating NBI power, during the power ramp phases, for the two shots. In figure 3(c) and (d) the soft X–ray traces are shown, highlighting the sawtooth period behaviour during the power ramps. The time evolution of the sawtooth period for both discharges is plotted in figure 3(e) and 3(f). In both cases the sawtooth period increases during the power ramp, and, in the case of shot ♯ 53593, decreases correspondingly during the ramp-down phase. In figure 3(g) and 3(h) the terms involved in the first sawtooth crash condition, [equation (1)] are plotted. $\delta\hat{W}_{core}$ remains clearly below $0.4\,\omega_{Dh}\,\tau_A$, indicating that plasma conditions are such that fast particle stabilization of the ideal internal kink is indeed possible. In figure 3(i) and 3(l) we have plotted the quantities in equations (2) and (3a). The fact that $-\delta\hat{W}$ is always less than $0.5\omega_{*i}\tau_A$ indicates that the ideal kink mode was stable throughout these discharges. In both cases, and in all the other discharges we have analyzed, the time at which the sawtooth period starts to increase corresponds to the time at which the fast ion stabilizing contribution is such that $-\delta\hat{W}$ becomes smaller than $-\hat{\rho}$, thereby stabilizing the resistive internal kink mode. Corresponding agreement is found during the ramp–down phase in the case of shot ♯53593. In this analysis effects on magnetic shear due to rapid time variations in the current profile are neglected, and the analysis cannot therefore explain every detail of the sawtooth period behaviour. In particular, transient current profile modifications could account for the sawtooth period variations observed during the power flat top phase in shot ♯53593. In the first part of the heating phase, before the power ramp, with either purely ohmic heating [shot ♯53593] or with very low auxiliary heating power [shot ♯50725], the sawtooth period remains almost constant, around 100 ms. In our picture this is the signature of a situation in which equation (3a) is already satisfied during the sawtooth ramp, and the crash is triggered by the fulfillment of equation (3b), when the magnetic shear s_1 exceeds the critical shear $s_{1\,crit}$ [equation (7)]. In this case the term $\delta\hat{W}_{fast}$ does not play any role in determining the sawtooth period. During the NBI power ramp, with the consequent increase of the fast ion pressure, $-\delta\hat{W}$ drops strongly below $-\hat{\rho}$, due to the growth of the term $\delta\hat{W}_{fast}$. At this point, the condition determining the sawtooth period is switched from equation

(3*b*), involving the critical shear [equation (7)], to equation (3*a*), i.e.$-\delta\hat{W} > -\hat{\rho}$, and it is the $\delta\hat{W}_{fast}$ term, being the dominant contribution to the kink energy, which directly determines the sawtooth period. This accounts for the linear correlation experimentally observed between the sawtooth period and the fast particle energy content inside the $q = 1$ surface.

In order to test this hypothesis we have carried out sawtooth period simulations with PRETOR. These simulations were performed with density profiles taken directly from experimental measurements, and kept constant during the sawtooth evolution. This approximation is consistent with analysis of the interferometer central line–integrated density signals, which in general do not show a strong signature of sawtooth activity, particularly during the H–mode phases. It thus appears that sawtooth relaxations in these discharges did not significantly affect density profiles, which were very flat inside the inversion radius. The experimental temperature profiles were simulated by adapting the values of transport coefficients, in order to reproduce correctly the experimental pressure profiles: this is crucial for a reliable evaluation of all the contributions to the kink energy. Particular care must be taken on this point, since an L–H transition usually occurs during the power ramp. The sawtooth period behaviour was nevertheless unaffected by this event. We have analyzed shots that remained in L–mode, such as shot ♯53593, shots in which the L–H transition occurred after the phase characterized by an increase of the sawtooth period, and shots in which the L–H transition clearly occurred before the beginning of that phase, such as shot ♯50725. In this last example the L–H transition occurred at 67.58 s: from figure 3 it is apparent that the sawtooth period increased only during the H–mode phase. No significant differences in the sawtooth period behaviour were observed in all these different situations.

The plasma current density and safety factor profiles in PRETOR are computed by solving a diffusion equation for the poloidal magnetic field, in which the plasma conductivity is assumed to be neoclassical and computed using formulae which take into account collisionality and plasma shape effects at finite aspect ratio [35]. The 1D transport code is coupled, at each time step, with a self-consistent equilibrium solver. It must be emphasized that application of the sawtooth trigger conditions requires detailed knowledge of several quantities, which must be computed consistently. In particular, the time evolution of the current density and safety factor profiles, involving the radial position of the $q = 1$ surface, as well as the evolution of the pressure profiles, and their related gradients at $q = 1$, play a crucial role in the calculation of all the contributions to the kink potential energy functional. As indicated in the previous section, the fast ion pressure profile, as well as the NBI heating power source, were taken directly from the PENCIL output. We now concentrate on the power ramp–up phase of shot ♯50725. Figures 4, 5 and 6 show the results of the PRETOR simulations for three representative time slices: 67.0 s, in figure 4, during the phase in which the sawtooth period is still constant and sawtooth activity clearly repetitive; 68.6 s, in figure 5, at the middle of the NBI power ramp, during the phase of increase of the sawtooth period; and 70.5 s, in figure 6, at the top of the power ramp, with the longest sawtooth periods. Figures

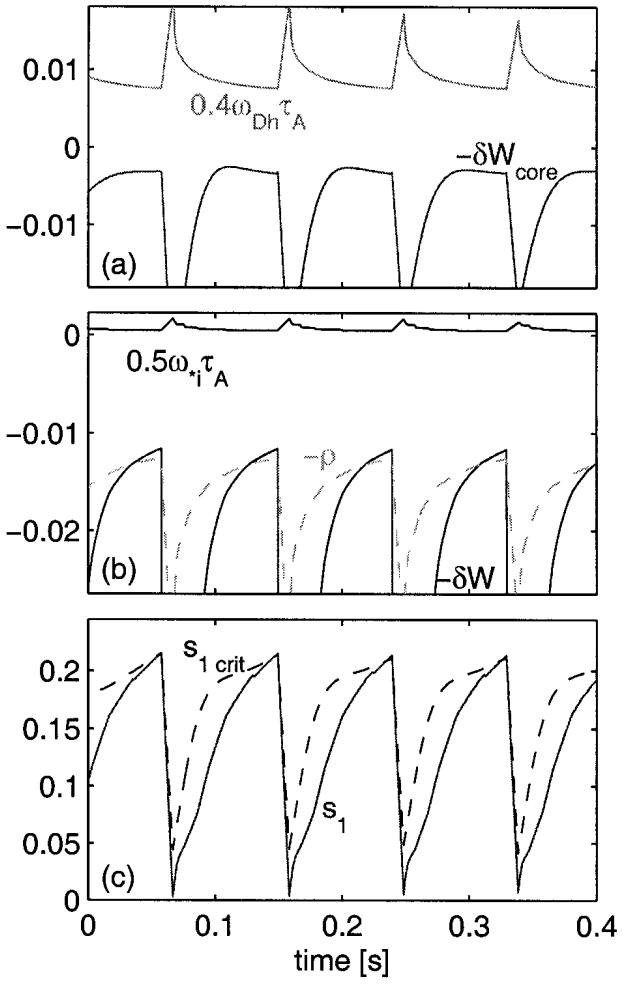

Figure 4. Time evolution of the relevant terms involved in the stability thresholds of the sawtooth period model in a PRETOR simulation of shot 50725 at time 67.0 s.

4(a), 5(a) and 6(a) show the time evolution of the terms involved in equation (1), while figures 4(b), 5(b) and 6(b) show the behaviour of the contributions of the kink energy and related stability thresholds for the terms involved in equation (2) and equation (3). In figures 4(c), 5(c) and 6(c) we show the time evolution of the magnetic shear s_1 and the critical shear $s_{1\,crit}$, equation (7).

At 67.0 s, figure 4, the $\delta\hat{W}_{fast}$ term is not yet large enough to be dominant in triggering the sawtooth crash. The condition $-\delta\hat{W} > -\hat{\rho}$ is reached during the sawtooth ramp before the shear s_1 crosses the critical shear $s_{1\,crit}$. In this situation it is equation (3*b*), or equivalently equation (7), which provides the triggering condition, and the destabilized mode is the resistive internal kink in the ion-kinetic regime. During this low NBI power heating phase, not only equation (1) is largely satisfied [figure 4(a)] but even $-\delta\hat{W}_{core}$ remains negative, showing that in this situation the ideal internal kink remains stable, independently of the stabilizing effect of fast particles.

At 68.6 s [figure 5], $\delta\hat{W}$ has not yet crossed $\hat{\rho}$ when s_1 crosses $s_{1\,crit}$. The condition

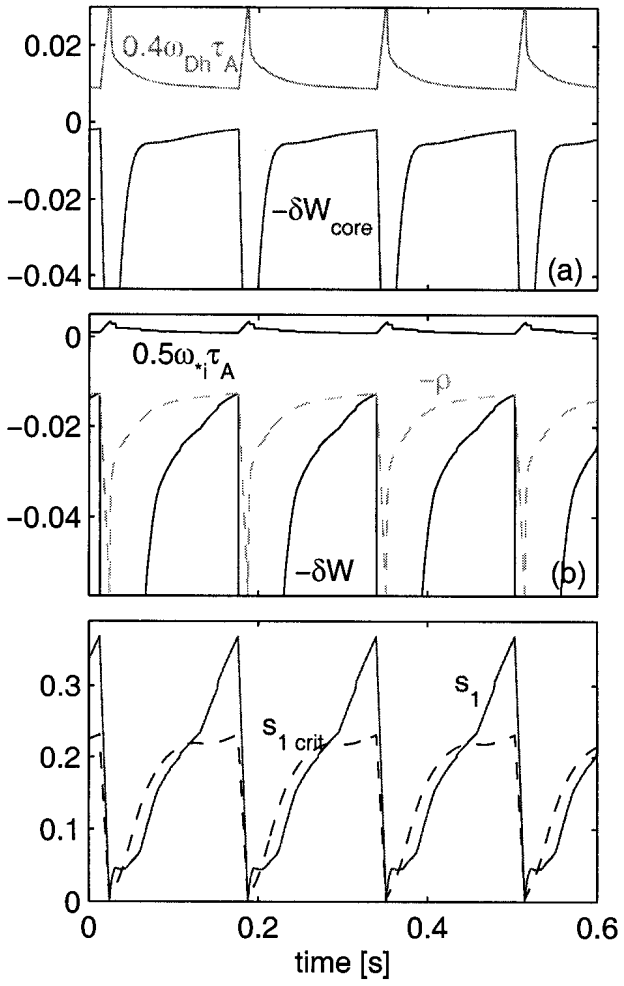

Figure 5. Time evolution of the relevant terms involved in the stability thresholds of the sawtooth period model in a PRETOR simulation of shot 50725 at time 68.6 s.

given by equation (7) [figure 5(c)] is clearly satisfied before $-\delta\hat{W}$ exceeds $-\hat{\rho}$, and hence no longer plays the dominant role in triggering the crash. In this case the condition $-\delta\hat{W} > -\hat{\rho}$ [equation (3a)] triggers the crash. The beam ion stabilizing term $-\delta\hat{W}_{fast}$, being the dominant contribution to the internal kink energy $-\delta\hat{W}$, thus plays the crucial role in determining the sawtooth period in the simulation, yielding a value of $\tau_{\rm saw}$ of 150 ms (the experimental value is 125 ms). The destabilized mode is still the resistive internal kink in the ion–kinetic regime. The ideal kink is stable, as shown in figures 5(a) and 5(b): equations (1) and equation (2) are both satisfied. Figure 5(a), in contrast to figure 4(a), shows also that the ideal internal kink would be close to instability without the stabilization provided by energetic ions, as $\delta\hat{W}_{core} \sim 0$ at the sawtooth crash.

At 70.5 s [figure 6] the behaviour is similar. The sawtooth crash is still determined by the condition $-\delta\hat{W} > -\hat{\rho}$ since equation (7) is satisfied earlier. In this case we note from figure 6(a) that the term $-\delta\hat{W}_{core}$ becomes positive during the sawtooth ramp, because of the strong NBI central heating and the consequent strongly peaked

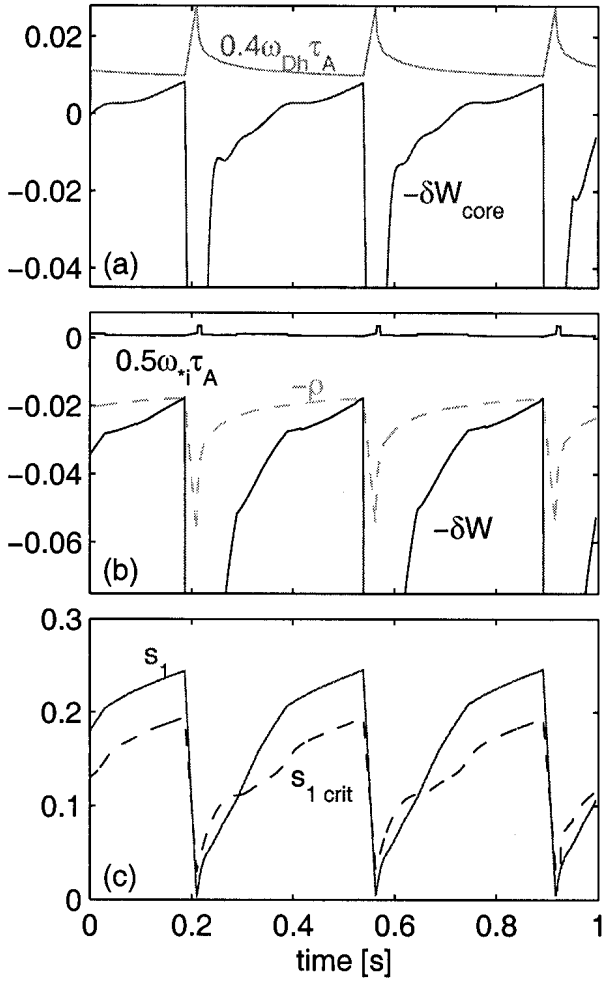

Figure 6. Time evolution of the relevant terms involved in the stability thresholds of the sawtooth period model in a PRETOR simulation of shot 50725 at time 70.5 s.

profiles. Without the fast ion stabilization, the ideal internal kink would be destabilized through equation (2) with $-\delta\hat{W} = -\delta\hat{W}_{core}$, after approximatively 160 ms, well before both the simulated crash, which occurs at $\tau_{\text{saw}} = 350$ ms, and the actual crash, which occurs after 325 ms. This strongly indicates the necessity of taking into account fast ion stabilization in order to explain experiments. Figure 6(a) shows also that at the time of the sawtooth crash the condition $\gamma_{core} \equiv -\delta\hat{W}_{core} / \tau_A < \omega_{Dh}$, which is necessary for fast particle stabilization, is satisfied only marginally. Thus, with strong NBI heating power, the consequent high ion temperature starts to destabilize more efficiently the ideal kink than the fast ions stabilizing effect, even if large fast ions densities are produced. The beam injection energy is then too low for beam ions to stabilize efficiently the internal kink. This indicates that the experiments have been performed in a stability window of parameter space, within which beam ion stabilization can be effective. The value of the shear s_1 at the crash is larger for sawteeth delayed by beam ion stabilization [figures 5(c) and 6(c)] than it is for the case in which s_1 is limited by s_{1crit} at the crash [figure

4(c)]. This may help to account for the excitation of NTMs in JET after long sawtooth periods, resulting from stabilization by NBI or ICRH [11].

With a completely analogous procedure, we have analyzed two other discharges and performed simulations at time slices with different levels of NBI power [see [1] for the complete analysis of another shot, ♯53595, not shown in the present paper]. The simulated sawtooth periods, determined by the triggering condition involving fast ion stabilization, as in the case of 68.6 s and 70.5 s for shot ♯50725 [figures 5 and 6], are found in every case to be in reasonable quantitative agreement, within 20%, with the experimentally observed sawtooth periods. In these discharges, the sawtooth period at the end of the NBI power ramp–up can be up to 5 times longer than the period at the beginning of the ramp.

6. Conclusions

Recent experiments in JET have clearly shown the stabilizing effect of fast ions arising from neutral beam injection on sawteeth. Heating power ramps have pointed out a linear relation between the sawtooth period and the fast ion energy content. Sawtooth periods up to 500 ms have been obtained with beam powers of less than 10 MW, about 5 times longer than those of the ohmic phase. A sawtooth period model, which takes into account two–fluid effects, finite Larmor radius effects, resistivity and fast particle stabilization, has been shown to be consistent with the experimentally observed time evolution of the sawtooth period. The beam ion contribution to the internal kink energy has been included in this model by means of a simplified expression assuming isotropic distribution functions. This expression has been validated with detailed calculations performed with the hybrid kinetic/MHD code NOVA–K, using realistic beam ion distribution functions calculated by the plasma analysis code TRANSP. The application of the sawtooth period model in a 1D transport code, PRETOR, coupled with a 2D equilibrium solver, has given sawtooth period simulations in good qualitative and quantitative agreement with the experimental observations: this allows a clear physical explanation of the observed phenomena and indicates that the main physical effects are well described by the theoretical model. It can be concluded that sawteeth were triggered by excitation of the resistive internal kink in the ion–kinetic regime. The relevant trigger condition, when beam ions are strongly stabilizing, is $-\delta\hat{W} > -\hat{\rho}$. The same criterion has been predicted to be applicable to burning plasmas with α–particle stabilization.

Acknowledgments

C.A. and O.S. would like to warmly thank F. Porcelli for helpful discussions. The authors wish to acknowledge the support of the UKAEA staff and Task Force M, in particular for diagnostic analysis. This work has been performed under the European Fusion Development Agreement and was supported in part by EURATOM, the Swiss

National Science Foundation, and the U.K. Department of Trade and Industry.

References

[1] Pochelon A *et al* 2001 *"Sawtooth stabilization by neutral beam–injected fast ions in JET"*, presented at *28th EPS Conference on Control. Fusion and Plasma Physics*, Madeira 2001, P5.009.

[2] Nave M F F *et al* 1998 in *Proc. 25th European Conf. on Control. Fusion and Plasma Physics*, (EPS, Prague 1998), ECA Vol **22C**, p. 365; submitted to *Nucl. Fusion.*

[3] Porcelli F, Boucher D, and Rosenbluth M N 1996 *Plasma Phys. Control. Fusion* **38** 2163.

[4] Campbell D J *et al* 1988 *Phys. Rev. Lett.* **60** 2148.

[5] Eriksson L-G, Mantsinen M *et al* 1998 *Phys. Rev. Lett.* **81** 1231.

[6] Porcelli F 1991 *Plasma Phys. Control. Fusion* **33** 1601.

[7] Graves J P *et al* 2000 *Phys. Rev. Lett.* **84** 1204.

[8] Duperrex P A, Pochelon A *et al* 1992 *Nucl. Fusion* **32** 1161.

[9] Ongena J *et al* 1990 in *Proc. 17th European Conf. on Control. Fusion and Plasma Heating*, (EPS, Amsterdam 1990), ECA Vol **14B**, Part 1, p. 383.

[10] Aymar R 2001 *Plasma Phys. Control. Fusion* **42** B385.

[11] Sauter O *et al* 2001 *"Neoclassical tearing mode seed island control with ICRH in JET"*, ibidem [1].

[12] Porcelli F *et al* 1988 *Report JET-IR(88)16 JET Laboratory.*

[13] Porcelli F *et al* 1993 *1992 Int. Conf. Plasma Phys. (Proc. Conf. Innsbruck, 1992)* Vol **16C**, part II, p. 901, (European Physical Society, Geneva 1993).

[14] Reimerdes H *et al* 2000 *Plasma Phys. Control. Fusion* **42** 629.

[15] Sauter O *et al* 1999 in *Theory of Fusion Plasmas*, Proc. Joint Varenna-Lausanne International Workshop, Varenna 1998, (J.W. Connor, E. Sindoni, J. Vaclavik, Eds), ISPP-18, Editrice Compositori, Bologna (1999), p. 403.

[16] Angioni C *et al* 2001 in *Theory of Fusion Plasmas*, Proc. Joint Varenna-Lausanne International Workshop, Varenna 2000, (J.W. Connor, O. Sauter, J. Vaclavik, Eds), ISPP-19, Editrice Compositori, Bologna (2001), p. 73.

[17] Budny R V, Bell M G, Biglari H *et al* 1992 *Nucl. Fusion* **32** 429.

[18] Gorelenkov N N, Cheng C Z, and Fu G Y 1999 *Phys. Plasmas* **6** 2802.

[19] Boucher D, Rebut P H 1993 in *Proc. IAEA Tech. Com. on Advances in Simulation and Modell. of Thermonuclear Plasmas*, 1992, Montreal(1993), p. 142.

[20] Howell D F, Buttery R, and Hender T, private communication.

[21] de Vries P *et al*, *"Analysis of shaping effects on sawteeth in JET"*, ibidem [1].

[22] Bussac M N, Pellat R, Edery D and Soulé J L 1975 *Phys Rev. Lett.* **35** 1638.

[23] Kruskal M D, and Oberman C R 1958 *Phys. Fluids* **1** 275.

[24] Cowley S C, Kulsrud R M and Hahm T S 1986 *Phys. Fluids* **29** 3230.

[25] Pegoraro F, Porcelli F,and Schep T J 1989 *Phys. Fluids B* **1** 364.

[26] Porcelli F and Migliuolo S 1986 *Phys. Fluids* **29**, 1741.

[27] Cheng C Z 1992 *Phys. Reports*, **211**, 1.

[28] Gorelenkov N N, Nave M F F *et al* 2000 *Effect of plasma rotation on sawtooth stabilization by beam ions*, presented at *27th EPS Conference on Control. Fusion and Plasma Physics*, Budapest 2000, ECA Vol. **24B** 1553.

[29] Putvinskij S V 1986 in *Reviews of Plasma Physics*, Vol.**18** (Kadomtsev, B. B., Ed.), Consultants Bureau, New York (1986) p. 239.

[30] Coppi B, Migliuolo S, Pegoraro F, and Porcelli F 1990 *Phys. Fluids B* **2** 927.

[31] McClements K G *et al* 1995 *Nucl. Fusion* **35** 1761.

[32] Dendy R O, Hastie R J, McClements K G, and Martin T J 1995 *Phys. Plasmas* **2** 1623.

[33] McClements K G, Dendy R O, Hastie R J, and Martin T J 1996 *Phys. Plasmas* **3** 2994.

[34] Bailey D 1998 *JET-R* (1998) 04;
Stubberfield P M and Watkins M L 1987 *JET-DPA(06)/87*;
Cox M 1984 *Culham report for JET KR5-33-04.*
[35] Sauter O, Angioni C, Lin-Liu Y R 1999 *Phys. Plasmas* **6** 2834.